Nanoelectronics and Its New Materials – A NEW ERA OF NANOSCIENCE

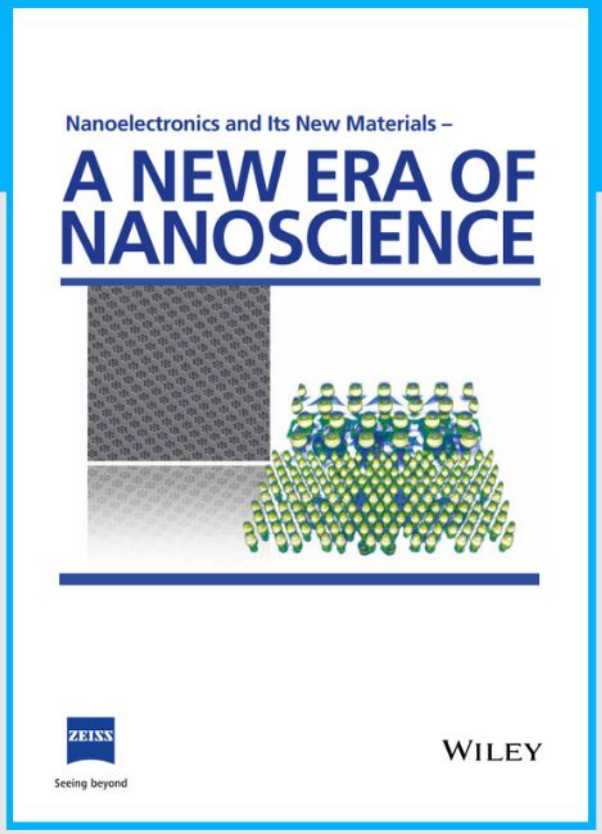

Discover the recent advances in electronics research and fundamental nanoscience.

Nanotechnology has become the driving force behind breakthroughs in engineering, materials science, physics, chemistry, and biological sciences. In this compendium, we delve into a wide range of novel applications that highlight recent advances in electronics research and fundamental nanoscience. From surface analysis and defect detection to tailored optical functionality and transparent nanowire electrodes, this eBook covers key topics that will revolutionize the future of electronics.

To get your hands on this valuable resource and unleash the power of nanotechnology, simply download the eBook now. Stay ahead of the curve and embrace the future of electronics with nanoscience as your guide.

ZEISS

Seeing beyond

WILEY

ADVANCED FUNCTIONAL MATERIALS
www.afm-journal.de

Bioresponsive, Electroactive, and Inkjet-Printable Graphene-Based Inks

Alessandro Silvestri, Alejandro Criado, Fabrizio Poletti, Faxing Wang, Pablo Fanjul-Bolado, María B. González-García, Clara García-Astrain, Luis M. Liz-Marzán, Xinliang Feng, Chiara Zanardi, and Maurizio Prato**

With the advent of flexible electronics, the old fashioned and conventional solid-state technology will be replaced by conductive inks combined with low-cost printing techniques. Graphene is an ideal candidate to produce conductive inks, due to its excellent conductivity and zero bandgap. The possibility to chemically modify graphene with active molecules opens up the field of responsive conductive inks. Herein, a bioresponsive, electroactive, and inkjet-printable graphene ink is presented. The ink is based on graphene chemically modified with selected enzymes and an electrochemical mediator, to transduce the products of the enzymatic reaction into an electron flow, proportional to the analyte concentration. A water-based formulation is engineered to be respectful with the enzymatic activity while matching the stringent requirements of inkjet printing. The efficient electrochemical performance of the ink, as well as a proof-of-concept application in biosensing, is demonstrated. The versatility of the system is demonstrated by modifying graphene with various oxidoreductases, obtaining inks with selectivity toward glucose, lactate, methanol, and ethanol.

1. Introduction

Since the past decade, a transition has been rapidly taking place in the field of electronics: devices are becoming smaller, thinner, flexible, and wearable.[1–4] Such a revolution is expected to replace traditional solid-state technology, which shows important limitations in terms of device flexibility, environmental concerns, and processing costs.[5] The development of increasingly efficient conductive inks is gradually facilitating this transition, because printing techniques offer low-cost, industrially appealing, and scalable alternatives for flexible electronics manufacturing.[6] The emerging role of conductive inks in a wide range of industrial applications is testified by the increasing number of published papers and patents and their growing market value share.[7]

A. Silvestri, A. Criado, C. García-Astrain, L. M. Liz-Marzán, M. Prato
Center for Cooperative Research in Biomaterials (CIC biomaGUNE)
Basque Research and Technology Alliance (BRTA)
Donostia-San Sebastián 20014, Spain
E-mail: asilvestri@cicbiomagune.es; mprato@cicbiomagune.es

F. Poletti, C. Zanardi
Department of Chemical and Geological Sciences
University of Modena and Reggio Emilia
Modena 41125, Italy

F. Wang, X. Feng
Faculty of Chemistry and Food Chemistry and Center for Advancing Electronics Dresden (cfaed)
Technische Universität Dresden
01062 Dresden, Germany

The ORCID identification number(s) for the author(s) of this article can be found under https://doi.org/10.1002/adfm.202105028.

DOI: 10.1002/adfm.202105028

P. Fanjul-Bolado, M. B. González-García
Metrohm DropSens
S.L. Vivero Ciencias de la Salud
C/Colegio Santo Domingo de Guzmán s/n, Oviedo 33010, Spain

C. García-Astrain, L. M. Liz-Marzán
Centro de Investigación Biomédica en Red
Bioingeniería
Biomateriales y Nanomedicina (CIBER-BBN)
Donostia-San Sebastián 20014, Spain

L. M. Liz-Marzán
Department of Applied Chemistry
University of the Basque Country
Donostia-San Sebastián 20018, Spain

L. M. Liz-Marzán, M. Prato
Ikerbasque
Basque Foundation for Science
Bilbao 48009, Spain

C. Zanardi
Institute of Organic Synthesis and Photoreactivity
National Research Council of Italy
Bologna 40129, Italy

M. Prato
Department of Chemical and Pharmaceutical Sciences
Universitá Degli Studi di Trieste
Trieste 34127, Italy

Indeed, conductive inks are extensively investigated in the manufacturing of organic light-emitting diodes (OLEDs),[8] solar cells,[9] flexible displays,[10] batteries,[11] radio-frequency identification (RFID),[12] thin-film transistors,[13] healthcare devices,[14] and sensors.[15] Several types of inks have been developed using metal (Ag, Au, Cu) nanoparticles, conductive polymers, and carbon allotropes.[7] Among these nanomaterials, graphene has received a great deal of attention, due to its exceptional carrier mobility (up to 2×10^5 cm^2 V^{-1} s^{-2}) and unique mechanical properties.[7] Furthermore, this 2D material can be exfoliated from graphite via solution processing with reduced costs and in mass production, making it an ideal candidate for the development of such inks.[16]

Several printing processes are compatible with graphene inks,[5] including: screen,[17] inkjet,[18] flexographic/roll-to-roll gravure,[19] and aerosol-jet printing,[20] and spray coating.[21] Among them, inkjet printing features many advantages, namely: simplicity, high repeatability, scalability, fast processing, and reduced costs.[15] However, the feasibility of inkjet printing is limited by fundamental ink properties such as viscosity and surface tension.[15,22–24] The development of the first classes of conductive graphene-based ink formulations did not consider the optimization of such parameters to match the requirements of the printing process, as the attention was focused on the efficiency of the exfoliation procedure and the quality of the graphene flakes.[25] Lately, new ink formulations have emerged, based on different organic or aqueous solvents.[24,26] The inclusion of additives in the formulation, such as polymers, cosolvents, and surfactants, has also been investigated, with the aim of optimizing the rheological properties and drying dynamics of the ink and even its interaction with the substrate.[25] We propose that the next challenge in the field is related to the development of graphene-based inks, capable of inducing selective interactions with target chemical species. This goal can be achieved by functionalizing graphene with organic functional groups or bioreceptors, thereby exploiting the large arsenal of chemical reactions that can be performed over graphene, ranging from covalent bonds to π–π interactions.[27] The transduction of the recognition event into a readable signal should result in inks that are responsive to a chemical stimulus (e.g., a change in concentration). Several examples can be found in the literature reporting graphene-based inks responsive to physical stimuli, such as temperature,[28–30] pressure,[30,31] or light.[32,33] Instead, only few inks have been reported with a well-defined response toward chemical stimuli, and they focus mainly on gas concentration,[34–36] pH,[37,38] and humidity.[39,40]

Herein, we present conductive inks, based on exfoliated graphene and oxidoreductase enzymes, which are selectively responsive to the concentration of biorelevant molecules. As an initial example, we employed glucose oxidase (GOx), covalently bound to electrochemically exfoliated graphene (EEG), as the recognition element: this enzyme can catalyze the oxidization of glucose into glucono-lactone, while producing H_2O_2. Cobalt phthalocyanine (CoPC) is added in the formulation to mediate the oxidation of hydrogen peroxide, thereby generating an electron flow that can be correlated to glucose concentration. The same system can be implemented for inks that are responsive to, e.g., lactate, ethanol, and methanol, by simply using enzymes specific for these substrates, thus rendering this technology highly versatile. We also demonstrated the successful modification and application of commercially available electrodes by inkjet printing.

2. Results and Discussion

2.1. Synthesis and Characterization of the Active Material

Engineering of graphene-based conductive inks requires the use of exfoliated graphene with reduced defect density and low degree of oxidation to ensure high conductivity.[41] Additionally, small flake lateral size is required to achieve colloidal stability and to avoid nozzle clogging during printing.[14] An inexpensive and readily scalable exfoliation procedure is also desirable to facilitate industrial production of the ink. Therefore, electrochemical exfoliation by application of an alternating current in *N,N*-dimethylformamide (DMF) was selected as the production method, followed by tip sonication at −4 °C for 30 min to control the lateral size of the flakes.[42] Electrochemical exfoliation is an industrially appealing method that can be readily scaled up by increasing the size of the graphite foils, as well as the volume of the electrochemical cell.[43,44] In these conditions, the resulting EEG is characterized by a median lateral size of 271 nm (measured from transmission and scanning electron micrographs (SEM and TEM); **Figure 1A–C**) and low oxygen content (6.2 at%, atomic percentage, by X-ray photoelectron spectroscopy (XPS); Figure 1D). The deconvolution of the C1s core peak in XPS shows that the graphene lattice is largely preserved (C=C contribution of 80.9 at%; Figure 1E); complete XPS characterization of our EEG is provided in Figure S1 in the Supporting Information. Analogously, the ratio between the D (1359 cm^{-1}) and G (1590 cm^{-1}) Raman band intensities of graphene (I_D/I_G), equal to 0.32 ± 0.05, confirms a low number of defects for small size exfoliated graphene, where the D peak mainly originates from the edges of the flakes (Figure 1F).[45] On the basis of atomic force microscopy (AFM) profiles (Figure S2, Supporting Information), we conclude that the produced EEG can be classified as few-layers graphene (≈10 layers).[46]

To produce an electroactive material, pristine EEG was modified with the bioreceptor GOx and an electrochemical mediator, CoPC, which, together with graphene, work as the signal transducer. We hypothesized that, by keeping all the components of the active material confined on the graphene flakes, the efficiency of the biocatalytic cycle should be strongly improved, in turn inducing a more sensitive response from the printed ink.[47] In fact, if GOx and CoPC are in close proximity, more rapid and efficient diffusion of the intermediate (H_2O_2) from one catalytic site to the other is expected. Preparation of such nanoconfined assemblies required chemical modification of pristine EEG with 4-phenylacetic acid diazonium tetrafluoroborate (**Figure 2**). The diazonium salt reacts with the graphene network via a single electron transfer (SET) mechanism, inducing a change in the carbon hybridization from sp2 to sp3.[27] The functionalized graphene (EEG–COOH) is characterized by free carboxylic acid groups on its surface, which play a double role: to help stabilizing graphene in water and to work as anchoring points for GOx in subsequent steps. CoPC was then incubated with EEG–COOH, so that it would adsorb over its basal plane. The adsorption and

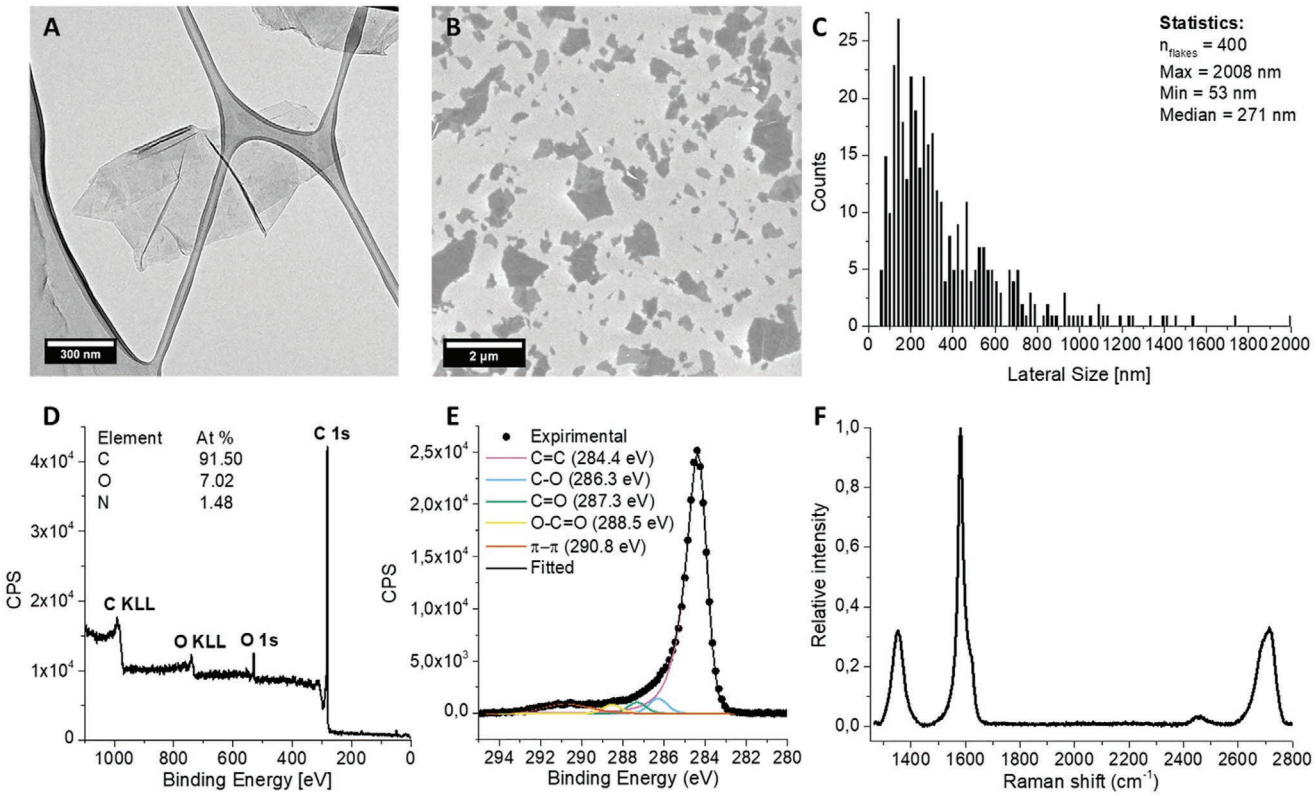

Figure 1. Characterization of EEG flakes. A) Representative TEM micrograph of a single EEG flake. B) SEM micrograph of EEG showing more representative information about the lateral size of the flakes. C) Statistical analysis of EEG lateral size from SEM micrographs (400 graphene flakes). The median value is 271 nm, with 2 µm and 53 nm as the maximum and minimum measured values, respectively. D) XPS survey spectrum highlighting the elemental composition of EEG. The material comprises mostly C (92.3 at%), with low percentages of O and N (6.2 and 1.5 at%) that indicate a low density of defects. E) High-resolution XPS spectra of the C1s core, which can be deconvoluted into five components: C=C (284.4 eV; 80.9 at%), C—O (286.30 eV; 4.7 at%), C=O (287.3 eV; 3.8 at%), O—C=O (288.5 eV; 2.7 at%), and π–π (290.8 eV; 8.2 at%). C=C is the dominating component of this core, confirming the low number of defects and thus a low degree of oxidation. F) Average Raman spectrum of EEG showing a low I_D/I_G ratio (0.32 ± 0.05).

self-assembly of CoPC on graphene were investigated in previous works and demonstrated to occur through π–π interactions.[48,49] Finally, GOx was covalently anchored onto free carboxylic groups through amidic coupling, by means of 1-ethyl-3-(3-dimethylaminopropyl) carbodiimide (EDC) and *N*-hydroxy succinimide (NHS) activation, thus obtaining EEG–GOx–CoPc.

Each step of the nanoassembly synthesis was characterized by XPS (**Figure 3**A–F; full characterization in Figures S3–S5 in the Supporting Information), thermal gravimetric analysis (TGA; Figure 3H), and TEM (Figure S6, Supporting Information). XPS survey spectra of EEG–COOH show an increase of the oxygen content from 6.2 to 13.8 at% (Figure 3A), as

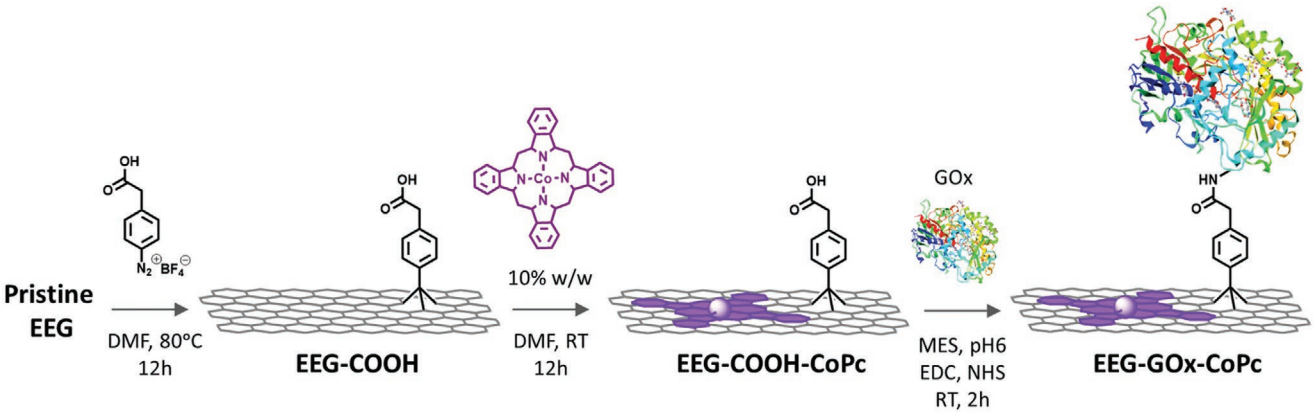

Figure 2. Synthetic scheme of the formation of the active nanoassembly included in the glucose-responsive ink.

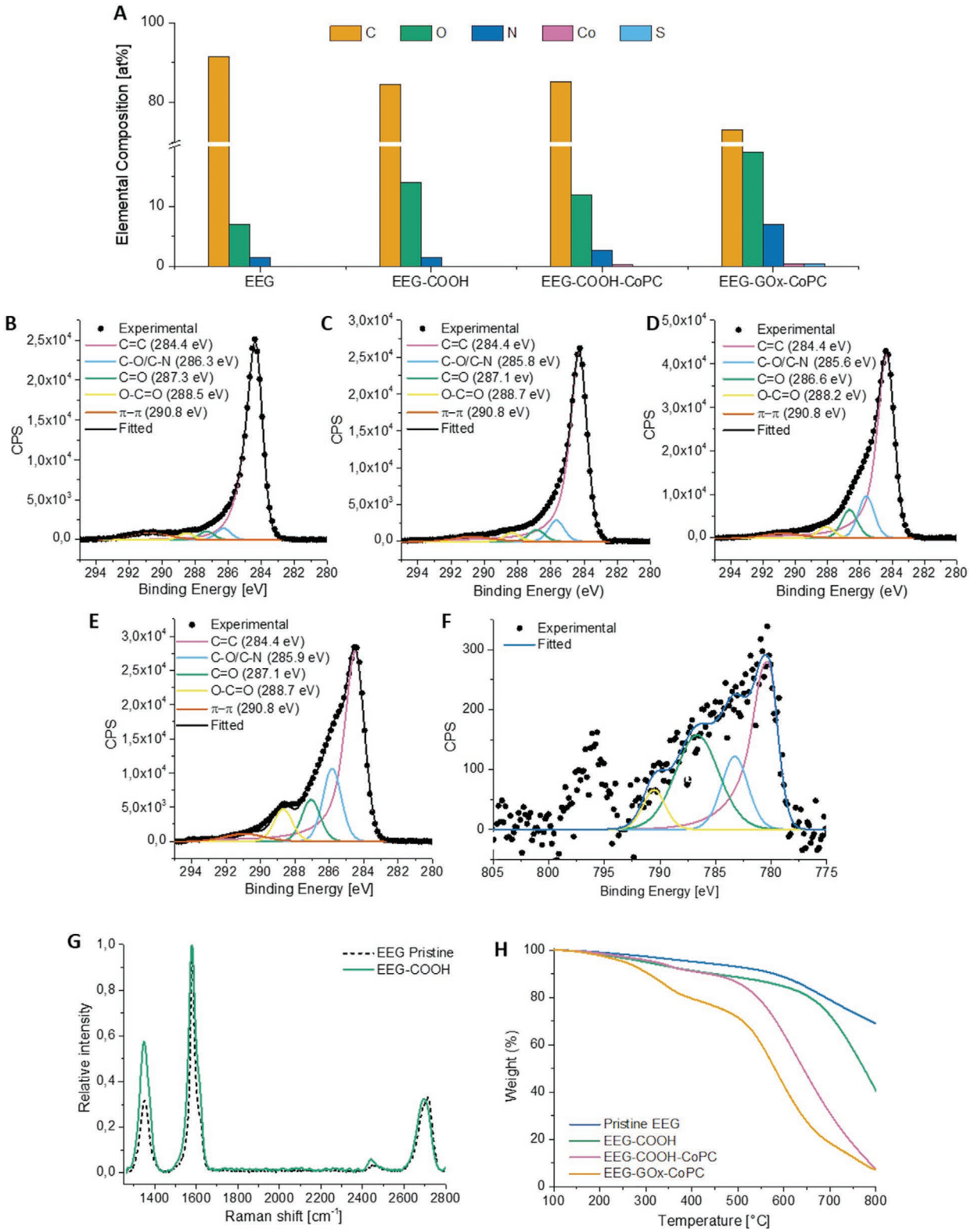

Figure 3. Stepwise characterization of the nanoassembly synthesis. A) Elemental composition of the material at the different stages of synthesis, obtained by XPS. High-resolution XPS spectra of the C1s core of B) EEG, C) EEG–COOH, D) EEG–COOH–CoPC, and E) EEG–GOx–CoPC, showing a gradual increase of carbon bonding with heteroatoms (O and N) in every step. The introduction of a large biomolecule (GOx) induced the most extensive change. F) High-resolution XPS spectra of the Co2p core of EEG–COOH–CoPC, which can be deconvoluted as Co(II). G) Superposition of the average Raman spectra of EEG and EEG–COOH, highlighting the enhancement in the I_D/I_G ratio after the SET reaction. H) TGA analysis of EEG, EEG–COOH, EEG–COOH–CoPC, and EEG–GOx–CoPC indicating subsequent weight losses after each functionalization stage.

compared to pristine graphene flakes, as well as an increment of all the components related to carbon–oxygen bonds in the C1s core (C—O, C=O, O—C=O) (Figure 3C), thereby confirming successful functionalization with the 4-phenylacetic acid moiety. Further evidence of the successful reaction is provided by the increased I_D/I_G ratio in Raman spectra, from 0.32 ± 0.05 to 0.56 ± 0.02 (Figure 3G), which indicates a change in C hybridization from sp2 to sp3 and the introduction of defects in the graphene lattice. Finally, TGA of EEG–COOH shows a weight loss (equal to 4.2%) between 200 and 500 °C, which is compatible with the loss of the organic functionalization (Figure 3H).

Likewise, EEG–COOH–CoPC was characterized by XPS. Upon CoPC adsorption, the N content increased by 1 at%, due to the presence of four nitrogen atoms in the phthalocyanine structure (Figure 3A). Furthermore, a peak appeared in the Co2p core, which can be deconvoluted as Co(II),[50] the expected oxidation state for this metal when coordinated to the PC (Figure 3F). The adsorption of CoPC on graphene flakes was confirmed by energy dispersive X-ray spectroscopy (EDX) in TEM (Figure S7, Supporting Information). On the other hand, TGA data show a marked weight loss starting from 500 °C, which is characteristic of CoPC (Figure 3H; Figure S8, Supporting Information). After coupling with GOx, the XPS survey spectrum of EEG–GOx–CoPC also shows evident changes: C and N contents strongly increased up to 19.1 and 7.0 at%, respectively, and a new peak appeared in the S2p core region (Figure 3A; Figure S5, Supporting Information). Additionally, the complexity of the high resolution C1s core was found to increase, showing a much stronger contribution from bonding of C with heteroatoms (Figure 3E). TGA of the final assembly clearly shows a double weight loss (Figure 3H); the first contribution being due to the loss of GOx and 4-phenylacetic acid, the second one to the decomposition of CoPC. Confirmation of amide bond formation and covalent functionalization of graphene with the enzyme was obtained through a control experiment: EEG–COOH–CoPC was incubated with GOx under the same conditions used for the amidation reaction, but without the coupling reagents (EDC, NHS). In their absence, the amount of adsorbed enzyme over graphene was found to be dramatically lower, and the electrochemical response (discussed below) of the final ink was feeble (Figure S9, Supporting Information).

2.2. Ink Formulation

Engineering of an inkjet-printable formulation requires some important parameters to be optimized. First of all, the solvent employed as the base for the ink should match viscosity and surface tension values within a certain range,[22–24] which is defined by the inverse Ohnesorge number (Z, Equation 1), commonly used to predict the printability of a formulation

$$Z = \frac{\sqrt{\gamma \rho \alpha}}{\eta} \tag{1}$$

where γ is the surface tension, ρ is the density, α the nozzle diameter, and η the viscosity. The ink is expected to produce stable drops when $1 < Z < 14$.[23]

Given that an enzyme is included in the ink formulation, we were constrained to use an aqueous solvent/base, more specifically phosphate-buffered saline (PBS) at pH 7.2, so that the activity of the biorecognition element is preserved. However, the Z value of pure water (for $\alpha = 20$ µm) equals 120, i.e., far away from the optimal range. Therefore, the use of additives and cosolvents was needed to improve rheological properties of the ink. *t*-Butanol and propylene glycol were added as cosolvents (10% v/v each) to decrease the surface tension (36.16 mN m^{-1} from pendant drop measurements; Figure S10a, Supporting Information) and to enhance the viscosity (2.14 mPa s from dynamic viscosity measurements; Figure S10b, Supporting Information), respectively. Low γ values help the formation of a Marangoni flow and reverse the coffee-ring effect, which may hinder the uniformity of the printed layer.[22] High η values avoid the formation of satellite drops, which might affect the lateral resolution of the printing process.[23] The inverse Ohnesorge number calculated for the described formulation ($Z = 8.9$) is below the maximum recommended value and predicts suitable printability.

Another important requirement of the ink formulation is that the mixture of solvent and cosolvent has a relatively high vapor pressure, so that the ink would dry sufficiently fast. The drying time of our selected formulation is of 1–4 h when exposed to air at RT (depending on the dispensed volume of ink), but it can be reduced to 5–10 min if stored in a desiccating chamber. The use of a desiccating chamber has the additional benefit of allowing fast drying of the ink at low temperature (up to 4 °C), again preventing degradation of the biorecognition element.

The colloidal stability of graphene flakes in the ink is another important parameter to be considered. ζ-potential values of -39.4 ± 5.1 mV (Figure S10d, Supporting Information) indicate a high surface charge, which is explained by the presence of numerous negatively charged groups (COO^-), which provide electrostatic stability to the flakes. Colloidal stability was additionally assessed by measuring the sedimentation rate of graphene in the ink through UV–vis spectroscopy (Figure S10e, Supporting Information). Stability of the suspension up to at least four hours was confirmed, which is compatible with inkjet printing.

The printability of the ink was assessed using filter paper as substrate, whose hydrophobicity was enhanced by treatment with 1% of polystyrene solution (in toluene). This printing substrate was chosen because it provides an excellent compromise between porosity, permeability, and printing resolution. In the first place, the contact angle of a 2.0 µL ink drop deposited over the substrate was compared with a solution of the active material in PBS (without cosolvents). The ink contact angle was reduced by half (62.35° vs 120.8°; Figure S11, Supporting Information), demonstrating that the formulation successfully reduced the surface tension and hindered coffee-ring formation upon drying (Figure S12, Supporting Information). Furthermore, the formulation improved the wettability of the ink, thereby facilitating its penetration into the paper and reducing the drying time (Figure S11, Supporting Information).

Then, to prove the feasibility of continuous printing, two different patterns were inkjet-printed on paper. Figures S13 and S14 in the Supporting Information display the Graphene Flagship logo and a graphene-like honeycomb structure printed

with the fully formulated ink and the active material in PBS. From optical microscopy images, it is clear that the formulation improved the homogeneity, continuity, and precision of the line. Using the setup and parameters described in this work, the definition of the printing process was equal to 60 ± 11 µm.

Finally, in our case, it is essential that the ink formulation be compatible with the enzyme, not affecting its activity. To evaluate the enzymatic activity of the ink, an electrochemical study was performed, as discussed in the following section.

2.3. Response of the Ink to Glucose Concentration

To evaluate the response of the ink to changes in glucose concentration, an electrochemical characterization was performed. The ink was drop-casted over a commercial carbon-based screen-printed electrode (C-SPE) and dried in a desiccating chamber at 4 °C. Cyclic voltammetry (CV) was then recorded incubating the modified electrode in PBS, in the absence (blank) and in the presence of 10.0×10^{-3} M glucose. In the presence of glucose, we observed a peak centered at +0.45 V, which can be ascribed to H_2O_2 oxidation, catalyzed by CoPC (**Figure 4A**).[48] The presence of H_2O_2 proves the enzymatic activity is maintained in the ink formulation. Amperometric measurements were performed in a flow injection analysis (FIA) setup, to evaluate the concentration-dependent response of the ink. The use of FIA presents several advantages, namely: it simulates the continuous application of a sensor, it provides an evaluation of the mechanical stability of the system under continuous flow, and it permits to randomize the analyte concentration, thereby ruling out any possible memory effect. A potential of +0.40 V was chosen to perform the amperometric measurements, as it would allow us to register significant oxidation current values without applying an excessive voltage. Ten different concentrations of glucose (from 0.1×10^{-3} to 50×10^{-3} M) were injected in a PBS flow-stream and run in triplicates (Figure 4B). No significant fluctuations in current intensity were registered for consecutive injections, which confirms a reliable response of the setup. The observation of sharp peaks indicates a rapid response to concentration changes (9.1 ± 0.6 s), as well as a fast recovery time. The baseline was found to be flat and characterized by a low noise level (8.3 nA). The device presents a linear response against glucose concentration, in the range of 0.1×10^{-3} to 10.0×10^{-3} M (Figure 4C). The sensitivity of the system was determined to be 0.26 µA cm^{-2} mM^{-1}, with a limit of detection (LOD) of 8×10^{-6} M, calculated as three times the standard deviation of the signal in the absence of analyte (Table S1, Supporting Information). The repeatability of the measurements was evaluated by performing three consecutive calibrations over the same electrode and then comparing the resulting electrode sensitivities (Figure S15A, Supporting Information). The calculated relative standard deviation (RSD) was below 10%, a value that is considered as acceptable for commercial C-SPEs, thereby confirming the stability of the

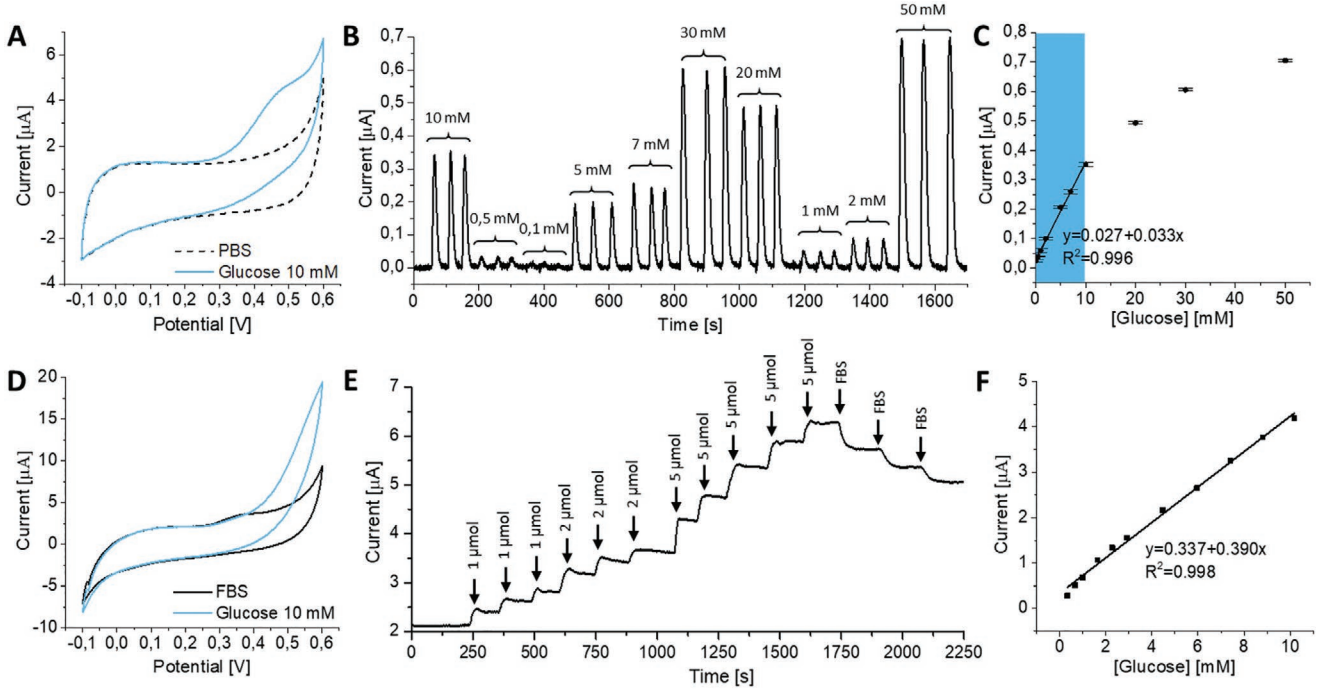

Figure 4. Electrochemical sensing of glucose concentration. A) CV responses obtained with ink drop-casted over a C-SPE in PBS, in the absence (dashed black line) and in the presence (solid blue line) of 10.0×10^{-3} M glucose (scan rate 20 mV s^{-1}). B) Representative FIA response obtained from the ink deposited on a C-SPE. Ten different glucose concentrations were tested, namely, 0.1×10^{-3}, 0.5×10^{-3}, 1.0×10^{-3}, 2.0×10^{-3}, 5.0×10^{-3}, 7.0×10^{-3}, 10.0×10^{-3}, 20.0×10^{-3}, 30.0×10^{-3}, and 50.0×10^{-3} M ($E = +0.4$ V, flow rate = 1 mL min^{-1}). C) Trend of the current measured in FIA versus glucose concentration. A linear regime was found between 0.1×10^{-3} and 10.0×10^{-3} M. Error bars represent the standard deviation among three injections in the same analysis. D) CV of ink drop-casted over a C-SPE in FBS, in the absence (solid black line) and in the presence (dashed blue line) of 10×10^{-3} M glucose (scan rate 20 mV s^{-1}). E) Representative amperometric analysis performed at $E = +0.40$ V with increasing/decreasing concentration of glucose in FBS. F) Trend of the current intensities registered in amperometric analysis, as a function of glucose concentration.

EEG–GOx–CoPC system. Reproducibility was tested by performing calibrations on three different electrodes, from which small variations in the sensitivity were registered, with an RSD as low as 3.6% (Figure S11B, Supporting Information). Finally, we evaluated the shelf-life of the ink (once dried on the electrode). No significant changes in the sensitivity were observed for 14 days after deposition, whereas after one month, the sensitivity was reduced by half (Figure S16, Supporting Information).

Both the linear range and sensitivity of the ink match the expected glucose concentrations in blood (2×10^{-3} to 30×10^{-3} M), sweat (0.02×10^{-3} to 0.6×10^{-3} M), tears (0.1×10^{-3} to 0.6×10^{-3} M), and condensed breath (0.4×10^{-3} to 4.0×10^{-3} M),[51] demonstrating the potential of the developed ink toward quantifying this metabolite in biological fluids. To assess the applicability of the ink in complex biological matrices, CV and amperometric analysis were performed in fetal bovine serum (FBS). It was observed that, for CV performed in FBS, the H_2O_2 oxidation peak is not so well defined as that obtained in PBS, but still a current increase could be detected in the presence of glucose (Figure 4D). In this case, more conventional amperometric analysis at increasing concentrations of glucose in the test solution was preferred, as it allows to squander less FBS in flow (Figure 4E). This analysis confirmed the stable baseline and resulted in a stairway profile, with increments proportional to the added amount of glucose. The linear range did not change with respect to that obtained in PBS (Figure 4F).

To prove our hypothesis that the efficiency of the biocatalytic cycle could be strongly improved by confining all the components of the active material on the graphene flakes, we run a control experiment. The same amount of CoPC present in the ink (calculated by TGA) was directly adsorbed over the C-SPE surface, rather than on the graphene flakes (Figure S17A, Supporting Information), so that it would be separated from other system components and therefore avoiding the nanoconfinement effect. Interestingly, the CV response of this control system showed a feeble H_2O_2 oxidation peak, which indicates a low efficiency of the catalytic cycle (Figure S17B, Supporting Information). Additionally, the slope in the linear range, and thus the sensitivity of the control electrode, was reduced to 1/3 with respect to the EEG–GOx–CoPC ink. We propose that this positive effect is due to the nanometric distance between GOx and CoPC, which favors the rapid and efficient diffusion of H_2O_2 from one component to the other, thereby improving the sensitivity of the method (Figure S17C, Supporting Information).[47]

An additional control experiment was carried out to check whether the addition of *t*-butanol and propylene glycol to the ink may affect the performance of the electrochemical detection. The electrodes were modified with a suspension of EEG–GOx–CoPC in PBS, without addition of any cosolvent. The performance of these electrodes was then compared to that of the ones prepared with the full formulation. The ink with cosolvents was found to present much higher capacitive currents in CV, as compared to the ink prepared in bare PBS (Figure S18A, Supporting Information). Even if a lower capacitive current would be preferred, the current peak at +0.45 V, generated in the presence of glucose from the electrodes modified with the complete formulation, is much more intense than that of the control. We propose that the presence of residual propylene glycol can reduce the hydrophobicity of the deposited graphene, thereby facilitating the diffusion of water and glucose through the flakes and reaching more units of covalently bound GOx. Our hypothesis is additionally supported by the wider linear range shown by the electrodes modified with the complete ink, compared to the controls (Figure S18B, Supporting Information): the earlier saturation of the control points toward a lower amount of GOx units being available to oxidize glucose. A final control experiment was performed by depositing GOx and CoPC directly over the C-SPE, without graphene. The sensitivity determined for this electrode was 0.067 μA cm^{-2} mM^{-1}, four times lower than that of the electrode modified with the graphene ink (Figure S19, Supporting Information), thus demonstrating the crucial contribution of this nanomaterial to improve the analytical performance of the ink.

2.4. Ink Versatility through Enzyme Variation

With the aim of demonstrating the versatility of the proposed technology, we conjugated EEG–COOH–CoPC with two different oxido-reductase enzymes: lactate oxidase (LOx) and alcohol oxidase (AOx) (Figures S20 and S21, Supporting Information). In this manner, we obtained graphene-based inks that were specifically responsive to lactate, MeOH and EtOH. The selected analytes are of primary importance in a plethora of applications, e.g., in clinical, sport, toxicological, forensic, and fermentation technologies; consequently, great economic and scientific efforts have been put in the development of devices to detect these analytes.[52,53] Notwithstanding, these enzymes are less robust than GOx and thus a suitable test bench for the reliability of our ink.

The electrochemical responses of EEG–LOx–CoPC and EEG–AOx–CoPC inks are reported in **Figure 5** for lactate (Figure 5A–C), ethanol (Figure 5D–F) and methanol (Figure 5G–I) detection. In the CV responses obtained from the EEG–LOx–CoPC modified electrode, the peak for H_2O_2 oxidation is clearly visible in the presence of lactate at 10.0×10^{-3} M (Figure 5A). The response to nine different lactate concentrations was tested in FIA in a randomized manner. As a result, the concentration-dependent response was registered with a linear regime spanning between 0.05×10^{-3} and 0.5×10^{-3} M. The sensitivity of the system was determined to be 11.2 μA cm^{-2} mM^{-1}. Lower current values were generated by EEG–AOx–CoPC (Figure 5D,E,G,H), due to the lower enzymatic activity of AOx (5–15 units mg^{-1} for alcohol oxidase from *Candida boidinii* against ≥100 units mg^{-1} for glucose oxidase from *Aspergillus niger*). However, both methanol and ethanol could be detected in the range between 50×10^{-3} and 1.0 M. Even if not relevant for biomedical applications, this linear range may be useful, e.g., for the analysis of short chain alcohols in foodstuff. The negative peaks visible in FIA are due to the elevated MeOH and EtOH concentrations injected, which change the conductivity of the electrolytic medium, inducing a reduction of the current, immediately followed by an increase due to H_2O_2 oxidation. AOx can detect both MeOH and EtOH, as it is able to oxidize different primary alcohols, being more efficient with the ones bearing shorter aliphatic chains. The sensitivities of EEG–AOx–CoPC for EtOH and MeOH were 4.0 and 1.0 mA cm^{-2} mM^{-1}, respectively.

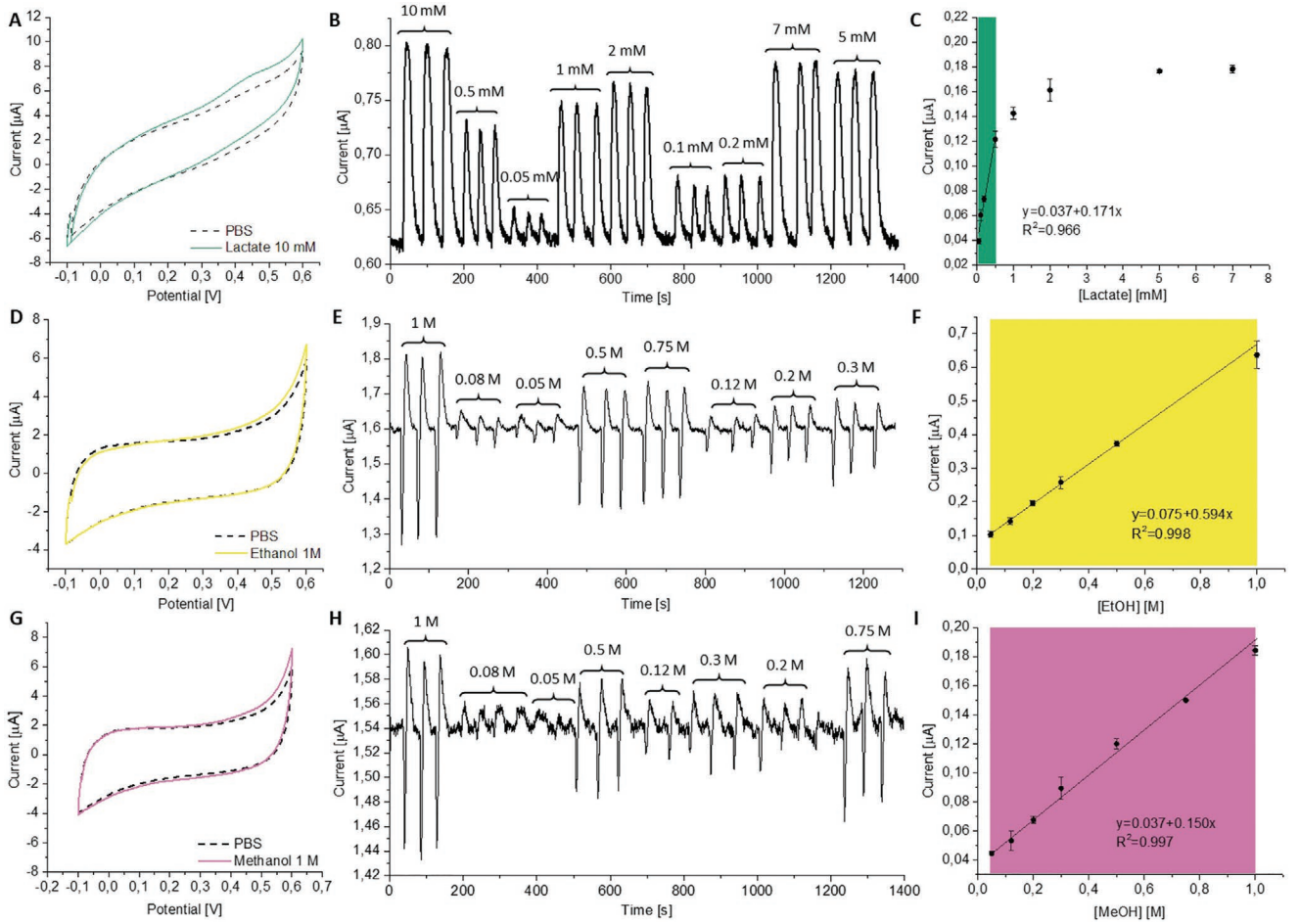

Figure 5. Electrochemical responses of inks produced with LOx and AOx. A) CV responses of EEG–LOx–CoPC inks deposited over C-SPE in PBS, in the absence and in the presence of 10×10^{-3} M lactate (scan rate 20 mV s^{-1}). B) Representative FIA response of EEG–LOx–CoPC ink deposited on C-SPE. Nine different lactate concentrations were tested, namely, 0.05×10^{-3}, 0.1×10^{-3}, 0.2×10^{-3}, 0.5×10^{-3}, 1.0×10^{-3}, 2.0×10^{-3}, 5.0×10^{-3}, 7.0×10^{-3}, and 10.0×10^{-3} M, in a randomized manner. C) Plot of the current intensities registered in FIA versus lactate concentration. The highlighted linear regime spans between 0.05×10^{-3} and 5.0×10^{-3} M. Error bars represent the standard deviation among three injections in the same analysis. D) CV responses of EEG–AOx–CoPC ink deposited over C-SPE in PBS, in the absence and in the presence of 1.0 M EtOH (scan rate 20 mV s^{-1}). E) Representative FIA response of EEG–AOx–CoPC ink deposited on C-SPE. Eight different EtOH concentrations were tested, namely, 0.05, 0.08, 0.12, 0.2, 0.3, 0.5, 0.75, and 1.0 M, in a randomized manner. F) Plot of the current intensities registered in FIA versus EtOH concentration. The highlighted linear regime spans between 0.05 and 1.0 M. Error bars represent the standard deviation among three injections in the same analysis. G) CV responses of EEG–AOx–CoPC ink deposited over a C-SPE in PBS, in the absence and in the presence of 1.0 M MeOH in PBS (scan rate 20 mV s^{-1}). H) Representative FIA of EEG–AOx–CoPC ink deposited on C-SPE. Eight different MeOH concentrations were tested, namely, 0.05, 0.08, 0.12, 0.2, 0.3, 0.5, 0.75, and 1.0 M, in a randomized manner. I) Plot of the current intensities registered in FIA versus MeOH concentration. The highlighted linear regime spans between 0.05 and 1.0 M. Error bars represent the standard deviation among three injections in the same analysis.

2.5. Modification of Electrode Surfaces by Inkjet Printing

Finally, we demonstrated that the proposed ink can be readily inkjet-printed and employed to modify electrode surfaces in an automated, scalable, and industrially appealing manner. To do so, we employed a multiple-head 3D bioprinter, with a dedicated head for inkjet printing (**Figure 6A**). Dispensing of the ink was controlled by means of air pressure and a piezoelectric valve. Using this technology, a C-SPE was modified within a few seconds with millimetric resolution, demonstrating the good printability predicted by the rheological properties. The ink was dried in 5 min at 4 °C in a desiccating chamber. The FIA recorded from the inkjet-printed electrodes confirmed that the ink preserved its enzymatic activity after printing and maintained all favourable electrochemical properties that were highlighted above (Figure 6B).

3. Conclusion

We have demonstrated the development of a graphene-based bioresponsive and electroactive inkjet-printable ink. The ink was obtained by modifying EEG with CoPC and covalently binding selected enzymes for the detection of analytes of primary importance: we typically developed three inks, with selectivity toward glucose, lactate, and simple primary alcohols, all of them with a good analytical performance. Electrochemical tests demonstrated that the enzymatic activity was maintained, and

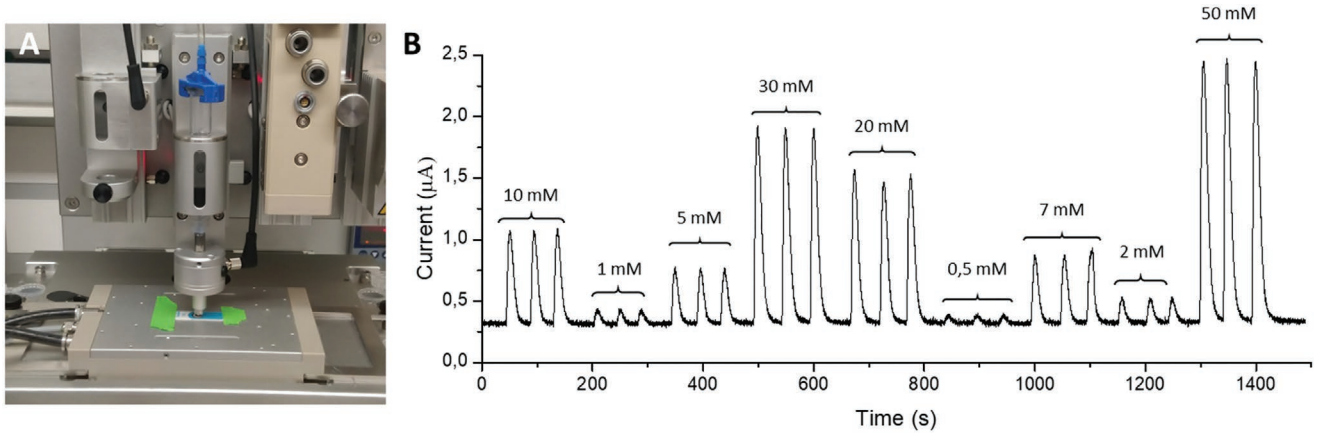

Figure 6. Modification of C-SPE by inkjet printing. A) Picture capturing the printing process over a C-SPE. B) Representative FIA response of the inkjet-printed EEG–GOx–COPc ink on a C-SPE. Nine different glucose concentrations were tested, namely, 0.5×10^{-3}, 1.0×10^{-3}, 2.0×10^{-3}, 5.0×10^{-3}, 7.0×10^{-3}, 10.0×10^{-3}, 20.0×10^{-3}, 30.0×10^{-3}, and 50.0×10^{-3} M, in a randomized manner.

C-SPE electrodes modified with the ink work in a continuous flow of the analyte solution, as well as in real complex matrices. The enhanced rheological properties of the water-based inks allow them to be printed using a scalable and inexpensive inkjet technology. Devices printed with these inks do not require any further postprinting treatment and can be used right away. Furthermore, the ink can be easily modified with other biorecognition elements (e.g., DNA and RNA fragments, cells, antibodies) and employed in the industrial production of different types of sensors. Other potential applications can be foreseen in the context of energy production, nanocapacitors, nanomotors, and nanoactuators, in which the transduction of concentration gradients in electron flow is of fundamental importance.

4. Experimental Section

Materials and Methods: Graphite foils were purchased from Alpha Aesar. EDC, NHS, GOx (*A. niger* EU ≥ 100 units mg^{-1}), AOx (*C. boidinii* EU = 5–15 units mg^{-1}), LOx (*Aerococcus viridans* EU ≥ 20 units mg^{-1}) EU, and CoPC were purchased from Sigma-Aldrich. Commercial reagents and solvents were used as received, without further purification, unless otherwise stated. Ashless filter paper 589/1 was purchased from Whatman. AFM characterization was carried out with Bruker Multimode 8 system using a tapping mode tip with a frequency of 320 Hz (Bruker TESPA-V2). The EEG suspension in isopropanol (0.1 mg mL^{-1}) was spin coated on freshly cleaved mica. Images were processed using WSxM 5.0. SEM characterization was performed using Zeiss Gemini 500 microscope, and the EEG isopropanol suspension (0.1 mg mL^{-1}) was deposited by spin coating on Si wafer. TEM micrographs were obtained using a JEOL JEM-2100F UHR electron microscope at 200 kV equipped with a TVIPS F-216 CMOS camera and UltimMax 80TSR EDX detector (OXFORD INSTRUMENTS), with 80 mm^2 SDD sensor and 127 eV resolution at 5.9 keV. Samples were prepared by drop-casting isopropanol solutions of the materials (0.1 mg mL^{-1}) on ultrathin carbon film-coated Cu-grids (Ted Pella Inc., USA) and drying it under ambient conditions. For EDX measurements, the areas over graphene flakes and areas of the carbon grid thin film were irradiated and the EDX spectra were collected. The image processing and statistics over the electron microscope micrographs were performed with Image J. XPS measurements were carried out using a SPECS SAGE HR 100 spectrometer in high vacuum (10^{-7} Pa), equipped with a nonmonochromatic X-ray source Mg with a Kα line of 1253.6 eV. An electron flood gun was used to neutralize for charging. XPS samples were prepared by drop-casting isopropanol materials suspensions (1 mg mL^{-1}) on glass slides coated with titanium. The spectra were processed and fitted with Casa XPS Version 2.3.16 PR 1.6. TGAs were performed under N_2 (flow rate 25 mL min^{-1}) using a TGA Discovery (TA Instruments). The samples were equilibrated at 100 °C for 20 min and then heated from 100 to 800 °C with ramp of 10 °C min^{-1} up to 800 °C. The data were processed with Trios version 3.3.1.4668. Raman spectra were recorded using a Renishaw inVia Raman microscope. Laser excitation wavelength of 532 nm, lens-based spectrometer with 1800 gr mm^{-1} gratings, Peltier-cooled front illuminated CCD camera (1024 px × 532 px), and a 100× objective were employed. Ink samples were prepared by drop-casting isopropanol solutions of the materials (1.0 mg mL^{-1}) on a glass slide and drying it under ambient conditions. Each spectrum is derived from the average of at least 300 spectra recorded in different spots of the sample for 5 s with a laser power of 1.29 mW. Data were processed using Ranishaw WiRE 4 software. The absorbance of the ink (0.25 mg mL^{-1}) at 660 nm was monitored through the time by UV–visible spectroscopy (Beckman Coulter DU 800 Spectrophotometer) for 4 h with measurements every 5 min. The relative % absorbance in respect to 0 min was used to evaluate the colloidal stability in time. The ζ-potential measurements of the ink (0.25 mg mL^{-1}) were conducted using a Malvern Nano ZS90 Zetasizer. Rheological properties were characterized using Physica MCR 302 rheometer (Anton Paar). All tests were carried out at 25 °C using 50 mm parallel plate geometry and a solvent trap to prevent water evaporation. The viscosity of the inks (1.0 mg mL^{-1}) was measured for shear rates from 100 to 1000 s^{-1}, with a gap equal to 1 mm. The viscosity of the ink at high share rates was calculated as average of the value between 500 and 1000 s^{-1}. Pendant drop and contact angle measurements were performed using DSA100 Kruss contact angle meter dispensing 2.0 µL drops and fitting with Young–Laplace equation. The obtained values were the average of ten measurements. Electrochemical characterizations were performed through CV and at constant potential with an electrochemical workstation Autolab MSTAT204 potentiostat/galvanostat (Metrohm). A multiheaded 3D Discovery bioprinter (RegenHU, Switzerland) equipped with inkjet printing head was employed to print the EEG–GOx–CoPC ink on C-SPEs (DRP110, Metrohm-Dropsens, ink concentration 1.0 mg mL^{-1}) and on filter paper treated with 1% polystyrene in toluene (ink concentration 50.0 mg mL^{-1}). The ink was dispensed by mean of air pressure (10 mBar) and a piezoelectric valve (300 µs opening-closure interval). A nozzle with an internal diameter of 100 µm was employed; 0.2 mm was selected as the distance between two deposited droplets. All samples were printed at room temperature. Once printed, the electrodes were dried in a desiccating chamber.

Electrochemical Exfoliation of Graphite: The electrochemical exfoliation process was performed in a two-electrode system, in which two graphite foils were used as cathode and anode in 0.1 M

tetra-*n*-butylammonium bisulfate (TBA·HSO_4) aqueous electrolyte. The pH value of the TBA·HSO_4 aqueous electrolyte was tuned by NaOH solution to nearly 7. The two graphite foils were placed in parallel with a constant distance of 2.0 cm. When an alternating current (±10 V, 0.1 Hz) was applied to trigger the exfoliation process, two graphite foils at both electrodes dissolved quickly accompanied by a violent eruption of bubbles. After the graphite foils immersed inside the electrolyte were entirely exfoliated, the exfoliated graphene flakes on top of the electrolyte were collected by vacuum filtration and then washed by water and ethanol. Finally, the wet graphene powder was dispersed in DMF via tip sonication (22 mm tip, 30% amplitude, 30 min) in an ice bath. The unexfoliated flakes and large graphene flakes were eliminated by centrifugation (3000 rpm, 10 min).

Synthesis of the 4-Carboxyphenyl Diazonium Tetrafluoroborate: 1 eq (5 mmol) of 4-aminophenylacetic acid (750 mg, 5 mmol) was dissolved in a solution of HBF_4 (2 mL, 32 mmol) in acetic acid (40 mL). Then, isoamylnitrate (2 mL, 12 mmol) was dissolved in acetic acid (20 mL) and added dropwise to the reaction mixture. The solution was stirred for 15 min at room temperature and subsequently quenched with Et_2O (30 mL). The reaction mixture was left overnight at −22 °C to allow the product to crystalize. The precipitate was filtrated and washed with ice cold Et_2O (60 mL). ^{1}H-NMR (400 MHz, MeOD, δ): 8.49(d, 2H, Ar H), 7.85 (d, 2H, Ar H), 3.91 (s, 2H, CH_2). IR (KBr): ν = 2297 cm^{-1} (s; ν(N≡N)).

Synthesis of the Nanoassemblies: EEG (50 mg) was dispersed in DMF (50 mL) and 4-carboxyphenyl diazonium tetrafluoroborate (500 mg) was added to the reaction mixture. The reaction was kept at 80 °C overnight. The product was filtrated over 0.1 µm PTFE membranes. The EEG–COOH was washed with DMF (2×), AcOEt (2×), MeOH (2×), acetone (2×), and Et_2O (1×), and left under vacuum to remove the solvent residues. EEG–COOH was resuspended in DMF (50 mL) and incubated with 10% of cobalt phthalocyanine (5 mg) for 12 h at RT. The obtained EEG–COOH–CoPC was filtrated over 0.1 µm PTFE membranes and washed with DMF until no CoPC was present in the washing solvent. The recovered EEG–COOH–CoPC was resuspended in MES buffer (0.5 M, pH 6) and sonicated for 5 min (sonicating bath). EDC (200 mg) was added and the mixture was sonicated for 5 min. NHS (125 mg) was added and the mixture was sonicated for 5 min. The corresponding enzyme (7.5 mg; GOx, LOx, AOx) was dissolved in MES buffer (5 mL) and added dropwise to the reaction mixture. The reaction was stirred at room temperature for 2 h. Finally, the product was dialyzed against PBS solution (Spectra/Por Float-A-Lyzers G2, cut-off 300 kDa).

Electrochemical Characterization of the Inks: For the electrochemical characterization, 5.0 µL of the inks with a concentration of 1.0 mg mL^{-1} was drop-casted over a C-SPE and dried in a desiccating chamber with silica gel at 4 °C. A layer of Nafion (1%, neutralized at pH 7) was deposited atop to avoid mechanical detachment of the nanomaterial during FIA analyses. CV was performed in the range of potential from −0.1 to +0.6 V at a scan rate of 20 mV s^{-1}. PBS, 0.1×10^{-3} M phosphate buffer at pH 7 enriched with 0.1×10^{-3} M of KCl was employed as electrolyte. For amperometric detection in FIA, a flow cell (Metrohm-Dropsens) was employed, coupled with a peristaltic pump and an HPLC injection valve (100 µL). Freshly prepared analyte solutions at different concentration levels were injected in a continuous flow of the electrolyte (1.0 mL min^{-1}). Three consecutive injections were performed for every concentration level. For the analysis of CA in FBS, fetal bovine serum (ThermoFisher Scientific) enriched with 0.1×10^{-3} M of KCl was employed as electrolyte medium. An electrolyte reservoir of 4.0 mL was established and let to circulate in the fluidic system in loop. Different volumes of a 50.0×10^{-3} M glucose mother solution were repeatedly added to the reservoir, gradually increasing the glucose concentration in the flux system. Calibration lines for the different analytes were obtained by plotting the obtained current intensity against the analyte concentration. Sensitivity of the sensor response was calculated from the slope in the linear range and normalized to the electrode area. LOD was calculated as three times the standard deviation of the signal in the absence of analyte (baseline).

Supporting Information

Supporting Information is available from the Wiley Online Library or from the author.

Acknowledgements

This work was supported by the European Commission (Spearhead project Chemsens, Graphene Flagship under Grant Agreement No. 696656). A.S., A.C., and C.G.-A. thank MINECO for their research grant (Juan de la Cierva Formacion/no. FJC2018-036777-I, Juan de la Cierva Incorporación/no. IJCI-2016-31113, and Juan de la Cierva Incorporación/no. IJC2019-040827-I, respectively). M.P., as the recipient of the AXA Bionanotechnology Chair, is grateful to the AXA Research Fund for financial support. This work was performed under the Maria de Maeztu Units of Excellence Program from the Spanish State Research Agency grant no. MDM-2017-0720.

Conflict of Interest

The authors declare no conflict of interest.

Data Availability Statement

Research data are not shared.

Keywords

biomolecules detection, enzymes, graphene, ink-jet printing

Received: May 26, 2021
Revised: September 4, 2021
Published online: October 5, 2021

[1] Y. Yang, W. Gao, *Chem. Soc. Rev.* **2019**, *48*, 1465.
[2] Y. Liu, M. Pharr, G. A. Salvatore, *ACS Nano* **2017**, *11*, 9614.
[3] P. D. Deepak, R. C. Nilesh, K. Do-Heyoung, P. Gomez-Romero, *Chem. Soc. Rev.* **2018**, *47*, 2065.
[4] W. Liu, M. Song, B. Kong, Y. Cui, *Adv. Mater.* **2016**, *29*, 1603436.
[5] T. S. Tran, N. K. Dutta, N. R. Choudhury, *Adv. Colloid Interface Sci.* **2018**, *261*, 41.
[6] D. Li, W. Lai, Y. Zhang, W. Huang, *Adv. Mater.* **2018**, *30*, 1704738.
[7] D. S. Saidina, N. Eawwiboonthanakit, M. Mariatti, *J. Electron. Mater.* **2019**, *48*, 3428.
[8] D. Han, Y. Khan, K. Gopalan, A. Pierre, A. C. Arias, *Adv. Funct. Mater.* **2018**, *28*, 1802986.
[9] H. Eggers, F. Schackmar, T. Abzieher, Q. Sun, U. Lemmer, Y. Vaynzof, B. S. Richards, G. Hernandez-Sosa, U. W. Paetzold, *Adv. Energy Mater.* **2019**, *10*, 1903184.
[10] N. Zhou, Y. Bekenstein, C. N. Eisler, D. Zhang, *Sci. Adv.* **2019**, *5*, eaav8141.
[11] S. Bellani, E. Petroni, A. E. Del Rio Castillo, N. Curreli, B. Martín-García, R. Oropesa-Nuñez, M. Prato, F. Bonaccorso, *Adv. Funct. Mater.* **2019**, *29*, 1807659.
[12] Y. Wang, C. Yan, S. Y. Cheng, Z. Q. Xu, X. Sun, Y. H. Xu, J. J. Chen, Z. Jiang, K. Liang, Z. S. Feng, *Adv. Funct. Mater.* **2019**, *29*, 1902579.
[13] S. Chung, K. Cho, T. Lee, *Adv. Sci.* **2019**, *6*, 1801445.
[14] S. P. Sreenilayam, I. U. Ahad, V. Nicolosi, V. A. Garzon, D. Brabazon, *Mater. Today* **2020**, *32*, 147.

[15] J. Li, F. Rossignol, J. Macdonald, *Lab Chip* **2015**, *15*, 2538.
[16] V. Nicolosi, M. Chhowalla, M. G. Kanatzidis, M. S. Strano, J. N. Coleman, *Science* **2013**, *340*, 1226419.
[17] W. J. Hyun, E. B. Secor, M. C. Hersam, C. D. Frisbie, L. F. Francis, *Adv. Mater.* **2015**, *27*, 109.
[18] S. Majee, M. Song, S. L. Zhang, Z. B. Zhang, *Carbon* **2016**, *102*, 51.
[19] E. B. Secor, S. Lim, H. Zhang, C. D. Frisbie, L. F. Francis, M. C. Hersam, *Adv. Mater.* **2014**, *26*, 4533.
[20] E. Jabari, E. Toyserkani, *Mater. Lett.* **2016**, *174*, 40.
[21] Z. Liu, K. Parvez, R. Li, R. Dong, X. Feng, K. Müllen, *Adv. Mater.* **2015**, *27*, 669.
[22] H. Hu, R. G. Larson, *J. Phys. Chem. B* **2006**, *110*, 7090.
[23] Y. Liu, B. Derby, *Phys. Fluids* **2019**, *31*, 032004.
[24] D. Mcmanus, S. Vranic, F. Withers, V. Sanchez-Romaguera, M. Macucci, H. Yang, R. S. K. Parvez, S. K. Son, G. Iannaccone, K. Kostarelos, G. F. C. Casiraghi, *Nat. Nanotechnol.* **2017**, *12*, 343.
[25] G. J. K. Hu, L. W. T. Ng, X. Zhu, R. C. T. Howe, C. G. Jones, M. C. Hersam, T. Hasan, *Chem. Soc. Rev.* **2018**, *47*, 3265.
[26] Y. Shin, Y. Shin, S. Vranic, X. Just-Baringo, S. M. Gali, T. Kisby, Y. Chen, A. Gkoutzidou, E. Prestat, D. Beljonne, I. Larrosa, K. Kostarelos, C. Casiraghi, *Nanoscale* **2020**, *12*, 12383.
[27] A. Criado, M. Melchionna, S. Marchesan, M. Prato, *Angew. Chem., Int. Ed.* **2015**, *54*, 10734.
[28] X. Gong, L. Zhang, Y. Huang, S. Wang, G. Pan, L. Li, *RSC Adv.* **2020**, *10*, 22222.
[29] T. Vuorinen, J. Niittynen, T. Kankkunen, T. M. Kraft, M. Mäntysalo, *Sci. Rep.* **2016**, *6*, 35289.
[30] M. Franco, R. Alves, N. Perinka, C. Tubio, P. Costa, *ACS Appl. Electron. Mater.* **2020**, *2*, 2857.
[31] A. Kaidarova, A. Kaidarova, M. A. Khan, M. Marengo, L. Swanepoel, A. Przybysz, C. Muller, A. Fahlman, U. Buttner, N. R. Geraldi, R. P. Wilson, C. M. Duarte, J. Kosel, *npj Flexible Electron.* **2019**, *3*, 15.
[32] R. F. Hossain, I. G. Deaguero, T. Boland, A. B. Kaul, *npj 2D Mater. Appl.* **2017**, *1*, 28.
[33] J. Zhao, Y. Zheng, Y. Pang, J. Chen, Z. Zhang, *J. Colloid Interface Sci.* **2020**, *579*, 307.
[34] T. Wu, A. De Luca, Q. Zhong, X. Zhu, O. Ogbeide, D. S. Um, G. Hu, T. Albrow-Owen, F. Udrea, T. Hasan, *npj 2D Mater. Appl.* **2019**, *3*, 42.
[35] V. Dua, S. P. Surwade, S. Ammu, S. R. Agnihotra, S. Jain, K. E. Roberts, S. Park, R. S. Ruoff, S. K. Manohar, *Angew. Chem., Int. Ed.* **2010**, *49*, 2154.
[36] L. Huang, Z. Wang, J. Zhang, J. Pu, *ACS Appl. Mater. Interfaces* **2014**, *6*, 7426.
[37] H. Bai, C. Li, G. A. Shi, *Chem. Commun.* **2010**, *46*, 2376.
[38] M. Fang, J. Long, W. Zhao, L. Wang, G. Chen, *Langmuir* **2010**, *26*, 16771.
[39] P. He, J. R. Brent, H. Ding, J. Yang, D. J. Lewis, P. O'Brien, B. Derby, *Nanoscale* **2018**, *10*, 5599.
[40] S. Santra, G. Hu, R. C. T. Howe, A. De Luca, S. Z. Ali, F. Udrea, J. W. Gardner, S. K. Ray, P. K. Guha, T. Hasan, *Sci. Rep.* **2015**, *5*, 17374.
[41] L. Vicarelli, S. J. Heerema, C. Dekker, H. W. Zandbergen, *ACS Nano* **2015**, *9*, 3428.
[42] K. Parvez, R. Worsley, A. Alieva, A. Felten, C. Casiraghi, *Carbon* **2019**, *149*, 213.
[43] F. Wang, Z. Liu, P. Zhang, H. Li, W. Sheng, T. Zhang, R. Jordan, Y. Wu, X. Zhuang, X. Feng, *Small* **2017**, *13*, 1702449.
[44] S. Yang, A. G. Ricciardulli, S. Liu, R. Dong, M. R. Lohe, A. Becker, M. A. Squillaci, P. Samorì, K. Müllen, X. Feng, *Angew. Chem., Int. Ed.* **2017**, *56*, 6669.
[45] C. Casiraghi, A. Hartschuh, H. Qian, S. Piscanec, C. Georgi, A. Fasoli, K. S. Novoselov, D. M. Basko, A. C. Ferrari, *Nano Lett.* **2009**, *9*, 1433.
[46] C. J. Shearer, A. D. Slattery, A. J. Stapleton, J. G. Shapter, C. T. Gibson, *Nanotechnology* **2016**, *27*, 125704.
[47] A. Rodriguez-Abetxuko, P. Muñumer, M. Okuda, J. Calvo, M. Knez, A. Beloqui, *Adv. Funct. Mater.* **2020**, *30*, 2002990.
[48] H. Wang, Y. Bu, W. Dai, K. Li, H. Wang, X. Zuo, *Sens. Actuators, B* **2015**, *216*, 298.
[49] P. Järvinen, S. K. Hämäläinen, K. Banerjee, P. Häkkinen, M. Ijäs, A. Harju, P. Liljeroth, *Nano Lett.* **2013**, *13*, 3199.
[50] M. C. Biesinger, L. W. M. Lau, A. R. Gerson, R. St, C. Smart, *Appl. Surf. Sci.* **2011**, *257*, 2717.
[51] E. W. Nery, M. Kundys, P. S. Jelen, M. Jo, *Anal. Chem.* **2016**, *88*, 11271.
[52] A. M. Azevedo, D. M. F. Prazeres, J. M. S. Cabral, P. Fonseca, *Biosens. Bioelectron.* **2005**, *21*, 235.
[53] G. Rattu, N. Khansili, V. Kumar, M. Prayaga, *Environ. Chem.* **2021**, *19*, 1135.